C.Beck, May 2010

Contents

1 Introduction

For the study of the solar oxygen abundance, we took data of the center-to-limb variation (CLV) in two spectral ranges at 777 nm and 557 nm, respectively, that contain a few oxygen lines. The spectra were obtained with the main spectrograph of the VTT. As context information and to distinguish between network and internetwork areas later, we obtained slit-jaw (SJ) images through a Ca II K Lyot filter. We completed CLV scans in both wavelength regions under medium to bad seeing condition; in addition, we observed some smaller active regions containing several pores in each wavelength range to obtain spectra from a cooler solar atmosphere. Some additional measurements for the determination of stray light were performed as well.

Table 1: *Left*: Orientation of the gratings for the two wl ranges. *Right*: Spatial and spectral sampling.

	Position grating	wl	focus
Predisperser	11500	557	27
Predisperser	8350	777	
Spectrograph	6194	557	91 mm
Spectrograph	6358	777	

	777 nm	557 nm
spectral	0.4635 pm	0.307 pm
spatial along slit	0.175”	0.174”
spatial scanning	0.176-0.180”	0.176-0.178”
SJ camera	0.166” x 0.166”	

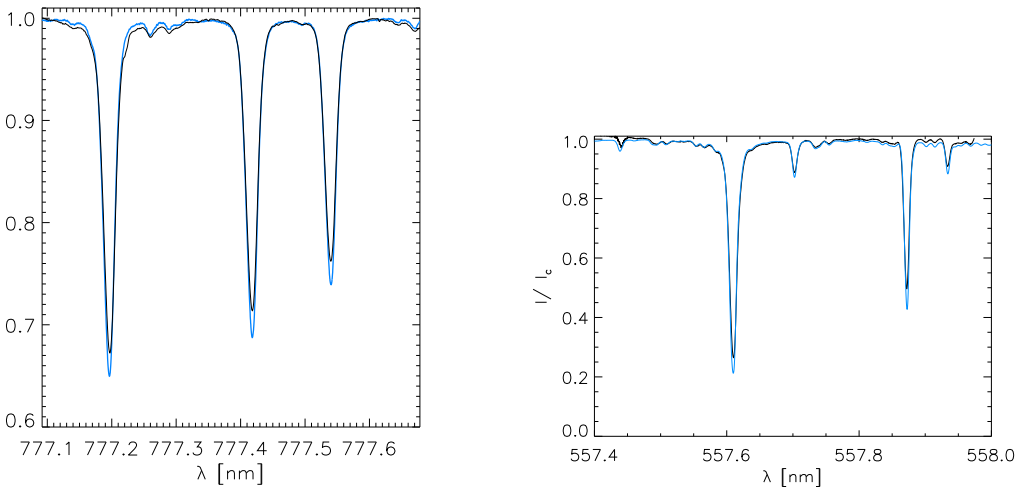

Figure 1: Average spectra on disc center at 777 nm (*left*) and 557 nm (*right*). *Black*: observations. *Blue*: FTS atlas.

2 Setup & observations

During an observing campaign at the VTT from 2009 Nov 15 until 2009 Nov 23, we obtained spectra around 777 nm and 557 nm. Both wavelength (wl) ranges contain some oxygen lines, the oxygen triplet around 777 nm and a forbidden oxygen line near 557.6 nm.

2.1 Spectra

We originally proposed to observe both wl ranges simultaneously using the predisperser of the main spectrograph with its low-order grating to obtain co-temporal spectra and to reduce the time needed for the observations. It, however, turned out that the wl ranges are separated slightly too much to fit through the predisperser. The spectra were vignetted on the last mirror before the predisperser focal plane. We thus had to observe them sequentially one after the other. The settings for the predisperser and main spectrograph to find the spectral lines are given in Table 1. We used a 40 micron slit (≡0.18”) to get the highest spectral resolution, and stepped it with 0.18” across the solar surface in the observations. The spectrograph was rotated to an angle of 226 degree to terrestrial North-South, to obtain a slit parallel to the East-West direction on the Sun (p0 ∼ 20 deg, image rotation due to position of C1 ∼ 20 deg). The slit orientation was cross-checked with SJ images at the EWNS limb on 19.11. and 21.11. . The system focus of the adaptive optics light path was set to -7.81 mm (value should not be valid the next time; optics inside the Fass was known to be seriously misaligned at that time).

The spectra were taken with the PCO 4000/2 camera (PCO 4000/1 is known to have strong fringes in the near-IR), mounted horizontally at the spectrograph output port. For finding the spectral lines, narrow-band prefilters at the desired wl ranges were inserted just behind the slit. Since the predisperser with the grating was used, the prefilters could be removed again after the camera was set up at the correct place. Even using the predisperser to preselect the wl range and spectrograph order, the 777 nm range at the spectrograph output port was found to be contaminated with light from a different spectrograph order; presumably the mask in the predisperser focal plane was slightly to wide. To suppress the false light, we used a color glass in front of the camera (RG 715, I believe Schott, contained in

a wooden box in one of the metal cupboards in the spectrograph room). The camera was used in 2x2 binning mode (tbc ?) with a restriction of the read-out area to the important spectral lines, giving around 1k x 1k images for 777 nm and 2k x 1k for 557 nm. Spatial and spectral sampling are listed in Table 1, they were derived from target scans and a comparison to FTS spectra (see Fig. 1). The spectral sampling gives the term "oversampling" a new meaning. We still have to cross-check with the corresponding equation, but I think we oversampled the theoretical resolution power of the spectrograph by a factor of 2-4. The wavelength scale in nm for using the data in IDL is something like: ll = 777.092+findgen(1266)·0.0004635 for 777 nm and ll = findgen(2004)·0.000307+557.359 for 557 nm.

Even if the PCO 4000-2 has less interference fringes in the near-IR at 777 nm than the other PCO, it still suffers from them. The *bottom left panel* of Fig. 2 shows an example spectrum after a standard gain correction to remove dirt and dust patterns on the slit and the CCD proper. The fringes can be clearly discerned. To remove them, three methods were tested: a 2nd order gain correction, spectral smoothing, and spectral Fourier filtering. For the 2nd order gain correction, all 199 gain corrected spectra of one scan were averaged. The resulting average spectrum can be assumed to be similar to standard flat field data, i.e. it should not contain any solar structure anymore. A correction matrix for the fringes was then derived. The application of this correction matrix, however, does actually not remove the fringe pattern, but instead increases it (*top right*). The reason is that the fringes are not stable in time, so the correction derived from the averaged spectrum introduces an additional fringe pattern. This method thus cannot be used. The second method used a spectral smoothing over 11 spectral pixels; the number was determined by trial-and-error. This approach effectively removes the fringe pattern, but also worsens the spectral resolution by smearing out the spectra (*bottom right*). The best result was obtained using a high-pass Fourier filter. The contributions of all spectral frequencies to a single spectrum below a limit of 6.4 pm were set to zero. This removes the fringe pattern while keeping the "sharpness" of the image (*top left*). The approach is visualized in the *right panel* of Fig. 2. The *upper part* shows the observed spectrum, FTS, and the spectra after correction by smoothing and high-pass filter. Both correction methods keep the shape of the spectral line while strongly reducing the fringes. The corresponding Fourier power as function of spectral frequency is displayed in the *lower part*. The origin of the fringe pattern can be clearly localized by two contributions near 0.2/pm and 0.3/pm (*black rectangles*). The high-pass filter was thus set as close as possible to the first contribution. From the shape of the power curve with frequency, this should not remove any significant information from the spectra, since the power already levels off to a constant value (≡ only white noise) at about 10 pm frequency. The thermal broadening of

$$\Delta\lambda = \sqrt{\frac{kT}{mc^2}} \cdot \lambda_0 \tag{1}$$

corresponds alone to 4.573 pm; unresolved velocities (e.g. macroturbulence) of 1 km/s would contribute additional 2.59 pm @777nm. The contribution of the spectrograph resolution should be determined also for completeness. I think that the high-pass filter thus does not cut any relevant solar information; I would recommend using this method.

By visual inspection it seemed that all of the oxygen lines are magnetically sensitive, they all showed a splitting effect in the pores, even the forbidden line at 557 nm.

The slit length corresponded to about 200", allowing us to do a full CLV on five overlapping positions. For the observations, we used a 150" spacing between consecutive positions to have a significant overlap in the maps.

2.2 Slit-jaw images

The VTT is equipped with a SJ camera system that offers three wavelengths: continuum imaging through a narrow-band interference filter, and two chromospheric channels in Hα and Ca II K using Lyot filters. Since for the later analysis it will be interesting to separate between locations without and with strong magnetic fields, we used the Ca II K channel to be able to identify at least the photospheric network. The SJ camera system unfortunately uses simply video cameras and only delivers low-quality images in jpeg format with a small dynamic range, read from the computer display of one computer with a frame-grabber card. The images additionally suffer from electronic interference fringes on the video cables. After one test using such jpeg images, we decided to mount the second PCO 4000-1 as SJ camera instead on 19.11.2009. The camera was fed by 50% of the light in the Ca II K channel, and triggered during the scanning simultaneous with the regular SJ using the RS232 trigger output. The exposure time was set early in the morning on QS at disc center; it turned out to be too long for later observations on active regions, thus some of the data is saturated on places with strong emission. Exposure times were reduced two times to 0.5 s and finally 0.3 secs. The image scale of the SJ camera was determined as 0.166" x 0.166" per pixel from a scan of the AO grid target.

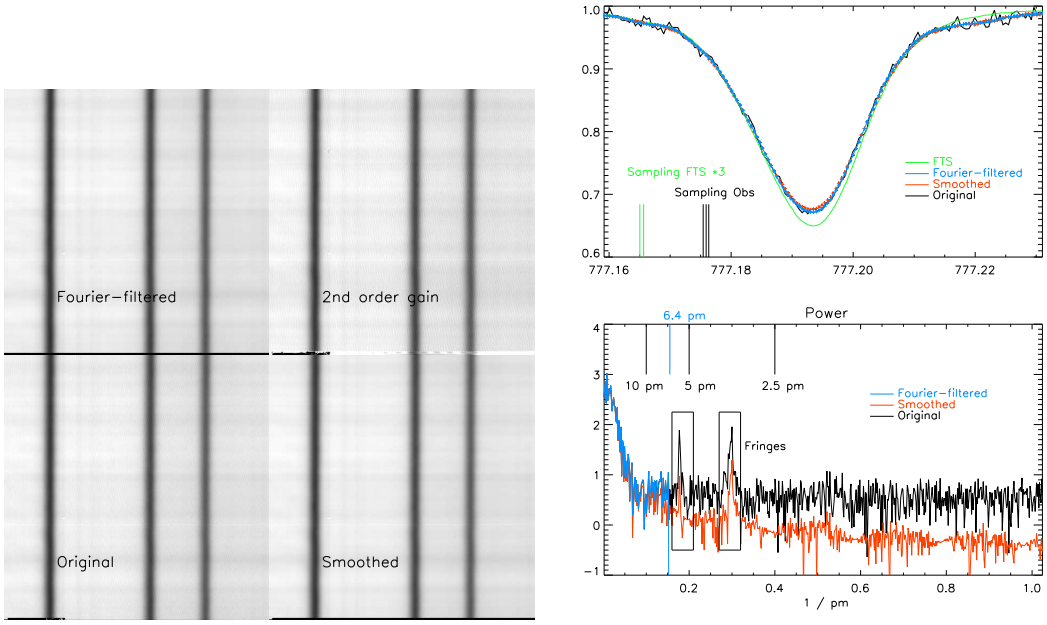

Figure 2: Fringes in the 777 nm data and their removal. *Left, counter-clockwise, starting left bottom*: original data after flatfielding, spectra after correction by smoothing, by 2nd order gain correction, by FFT filter. *Right top*: example spectrum. *Black*: original spectrum. *Red*: smoothing of width 11 pixel. *Blue*: high-pass filter. *Green*: FTS atlas. The *short vertical bars at bottom* denote the spectral sampling of FTS atlas (*3) and observations. *Right bottom*: Fourier power of the spectra above. The fringe pattern is due to the two frequency ranges marked with *black rectangles*. The high-pass filter was set to cut everything above a frequency of 6.4 pm.

The *leftmost image* of Fig. 3 shows one example of the SJ images from the 19.11 after readjusting the exposure time. This image was not flat fielded, it shows the slightly inclined slit (rotation angle to the CCD column: 2.9 degree), and the two hairlines. The *2nd column* shows the same image after flat field correction. The slit and the hairlines are nearly full removed by the gain table, even if faint traces of them are still left over. There appeared a slight complication that I did not think of before. During the flat fielding, the telescope is moving and the AO beamsplitter that does the spatial scanning is at the central position. This means that the field stop in the filter wheel is in the central position on the CCD. During the spatial scanning, the BS is tilted which moves the field stop image across the slit. Thus a gain table correction with a 135" radius is only available for the central position of the field stop, whereas the lit area during the scanning is displaced by up to $\pm \sim 40$" to the side. The location of the slit always is lit and always gets corrected by the gain table, but some other regions of (less) interest in the SJ image cannot be corrected. E.g., the hairlines appear again at x$\sim$ 70" in the flat fielded image. The effect does not affect the location of the slit, but of course could be avoided the next time by doing three flat fields for the SJ camera, with the BS at $\pm$ 50" and in its central position. The *3rd column* of the figure shows the resulting scan map, cutting out only one column at the approximate location of the slit for each scan step. A CCD column 10 (12) pixels away from the slit itself was taken, with the number in parentheses valid for all observations after the 19.11.09. The SJ scan maps thus are always displaced in x, and have to be shifted by 10 (12) pixels times the scan step width that was 0.18" and 0.36", respectively, for some maps. The shift is to the right when the original save files are used. The SJ image quality reflects the rather mediocre seeing conditions during the observation; even while locking on one of the pores, the AO jumped a few times. The same jumps are naturally also in the spectra, not only the SJ images, as the *4th column* shows. It was constructed from the continuum intensity value in the spectra themselves. Since seeing effects at a wavelength of 777 nm are much less than for Ca II K at 393 nm, the scan map from the spectra thus also has a higher spatial resolution.

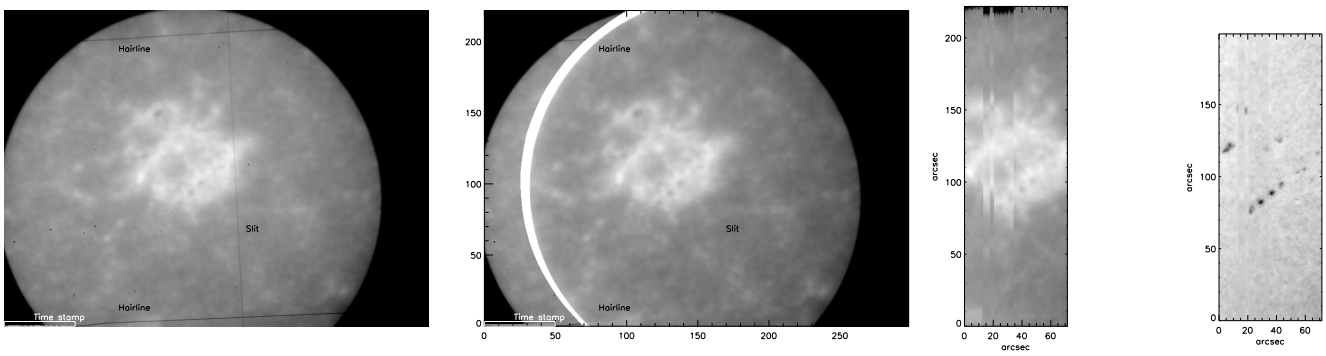

Figure 3: Example of the Ca II K SJs with the PCO camera (19.11.; UT 12:25) before (*left*) and after the flatfielding (*2nd column*); SJ scan map for the observation (*3rd column*) and scan map (*4th column*). AO lock point jumped a few times, thus the two scan maps do not fully fit to the single SJ image.

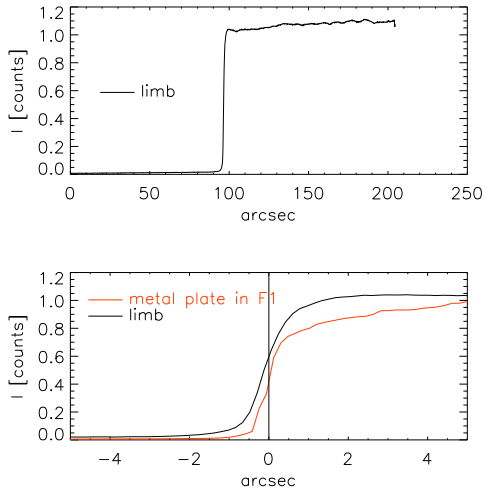

Figure 4: Observations in 777 nm with the slit across the limb and half of the FOV blocked by a metal plate in F1. *Top*: full spatial range across the limb. *Bottom*: magnification of the area near the limb (*black*) and near the edge of the metal plate (*red*), respectively.

2.3 Stray light measurements

A visual comparison of the observations with the FTS spectra in Fig. 1 suggests a rather low stray light level inside the spectrograph, the line depth differs only by few percent (3-5%). We did some additional measurements of straylight level, but after some thought they won't be important for the abundance study, since they rather deal with the spatial stray light, i.e. the effects on spatial resolution by scattered light throughout the telescope and the instrument. For the abundance study anyway spatially averaged spectra will be used, or "resolved" spectra where the resolution still is not critical, like for instance only doing a rough distinction between granules and intergranular lanes. I only included two of the measurements here, one with the slit crossing the limb, the second with a metal plate in the F1 telescope focal plane. Figure 4 shows the intensity variation along the slit for the two cases. The intensity in the occulted or unlit area drops to a residual of $<<10$ % on a few arcsecs; but as stated before, this measures the spatial variation of straylight.

For determining the straylight level *inside* the spectrograph, we have first to obtain a theoretical curve corresponding to the resolution of the spectrograph to see for how much this accounts for, and then we can apply the approach of Allende Prieto et al. 2004 (see Sect. 7 below). This will, however, only be important for the final comparison with theoretical spectra. A preliminary discussion of the other straylight measurements is available in a first order paper draft, it can be supplied if wanted. The tests done there showed that different approaches of treating the straylight basically only have any noticeable effect on the spectra close to the limb (up to ∼50" distance). Only the total intensity level of the profiles changed, the spectral shape was rather unaffected. For the abundance study, it may require again a closer investigation, since the line depth also varies with the global intensity level.

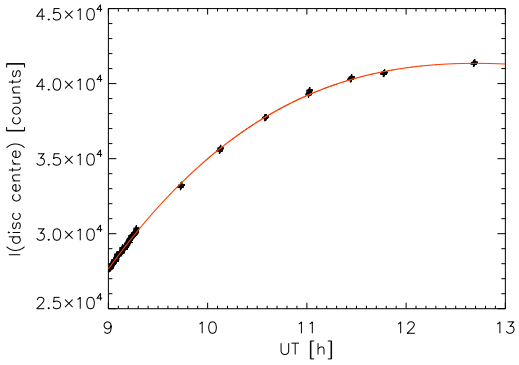

Figure 5: Intensity normalization curve for the morning of the 19.11.09.

3 Intensity normalization

The continuum intensity level in the observations changes by two sources: the light level in the telescope that changes with zenith distance, and the pointing on the solar surface. To facilitate a solid normalization of the observed intensity values and to be able to relate them finally to absolute energy units, we repeatedly took observations on disc center between the individual scan maps of the CLV. Figures. 5, 23, and 24 shows the result of such measurements for all days. By fitting a polynomial to these observations, they provide a value in counts as function of time that can be used to normalize any of the observed spectra relative to the intensity at disc center at the same instance. Since both spectral ranges contain continuum wavelength points, no further normalization step to, e.g., any atlas spectrum is required like for the POLIS Ca spectra.

4 Data alignment and exact locations

There are two approaches for determining the exact locations of the observations on the solar disk. The first is to use the pointing information of the VTT telescope control computer, the slit orientation, and the scanning step width. A routine for deriving the position of every scan step from this information is available. For 19.11.09, this delivered the plot shown in Fig. 6. The accuracy is limited by the correctness of the VTT pointing information. Since the observations were late in the year, and the first coelostat mirror was displaced by 90 deg to terrestrial North-South, the solar image in the focal plane of the VTT was rotated by about 20 deg. The image rotation limits the reliability of the VTT pointing information, since with such a large rotation angle the determination of the center of the disc with the find_center procedure gets important (huge leverage of offsets of the zero point). The positions may thus be off by some 10's of arcsec, but the values from this approach should suffice for any first order investigation. The position errors will only get critical near the limb. For the data of 19.11.09, the offset of the map at the limb was found by comparing the solar radius (972") of that day with the position attributed to the limb in the observation (∼1000"). All position values of the day were thus shifted by ∼ 20" in x to get a better match, but this offset in x (and also any in y) is not stable with time as well. The following points are of interest: a) the coverage in positions is complete due to the overlap; b) the chosen slit orientation gave ∼ an East-West orientation of the slit on the Sun.

A second method is to use the additional information provided by the full-disk images from Chrotel and/or MDI. Figure 7 shows the corresponding images in the Ca II K channel of Chrotel, the MDI magnetogram and the MDI intensity on the 19.11.2009. There were three active regions on the solar disk whose locations differ sufficiently to obtain a solid alignment between Chrotel and MDI (not yet done for the figure, this is simply cut & paste). The size of the solar disk in each case has been fit to match the reference disk by eye only; the image rotation of the Chrotel image has not yet been taken out (turret telescope); the match of solar radius and center location is imperfect; and the temporal difference between the MDI images and the observations is several hours. Thus the offsets between the overplotted observed FOVs and the full-disk images will significantly reduce. Note that the match to the Chrotel image is already quite good which is important, because the Chrotel image itself can be accurately aligned to the CA II K SJ images (Fig. 8) taken during the scans, down to localizing the slit exactly on the full-disk image including its orientation (cp. also with Fig. 3, the 4 small pores in a row can be identified well in each of the Figures). This allows to cross-check the position information from the VTT telescope control computer, and if necessary to ensure that we can precisely located the FOVs of the spectra finally relative to the MDI full-disk image.

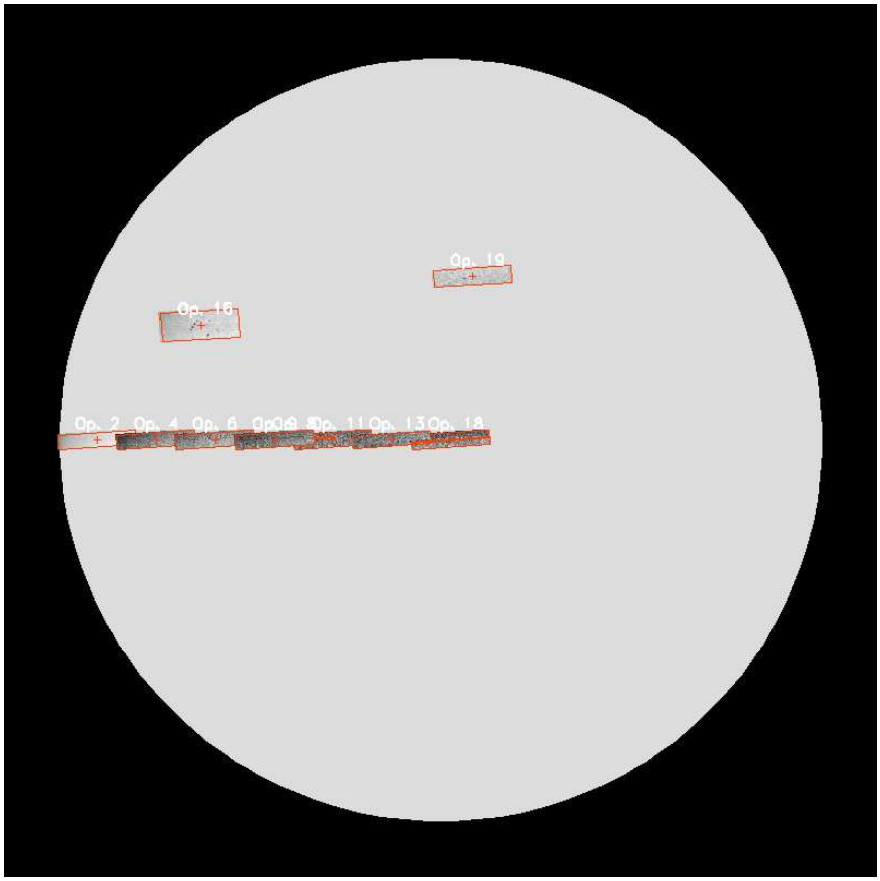

Figure 6: Location of the observed FOVs on the Sun on 19.11.09, overlaid over a full-disk reference image. Operation number is given at top, the *red rectangle* encloses the full scan area, the center of the FOV is given by the *red cross*.

N.B.: Chrotel data can be accessed from http://www3.kis.uni-freiburg.de/∼chrotel/, but the page is NOT YET OFFICIAL. I did not download all data for the days of our observations, only every third or so in Ca II K. We can use the data (since the poor PhD student responsible for Chrotel had just got his dissertation being corrected by me and owes me more than one favor from before already), but before any inclusion in a publication we might eventually have to contact the KIS officially to ask for permission. Thus, if you want to use the Chrotel data also for other days, do it, but don't submit anything with the data yet before the KIS has given green light. C.Bethge also is young and needs publications...

4.1 Positions 20.11.09, 557 nm

Figure 9 shows the locations of the FOVs for 20.11.09, when the wavelength was changed to 557 nm. The offset was determined using the map at the limb, it was again about 20". The coverage of CLV positions should be complete, the map at the very limb had to be done with some offset in y since there were no suitable faculae for locking AO at y∼0".

4.2 Positions 21.11.09, 557 nm

Figure 10 shows the locations of the FOVs for 21.11.09. The offset was set to 20" as the days before since no limb observations is available on that day. The value should be confirmed using the two observations of the active region (Op. 4 and 8).

4.3 Positions 22.11.09, 557 nm

Figure 11 shows the locations of the FOVs for 22.11.09. The offset was set to 20". The value should be confirmed using the observation of the active region (Op. 5).

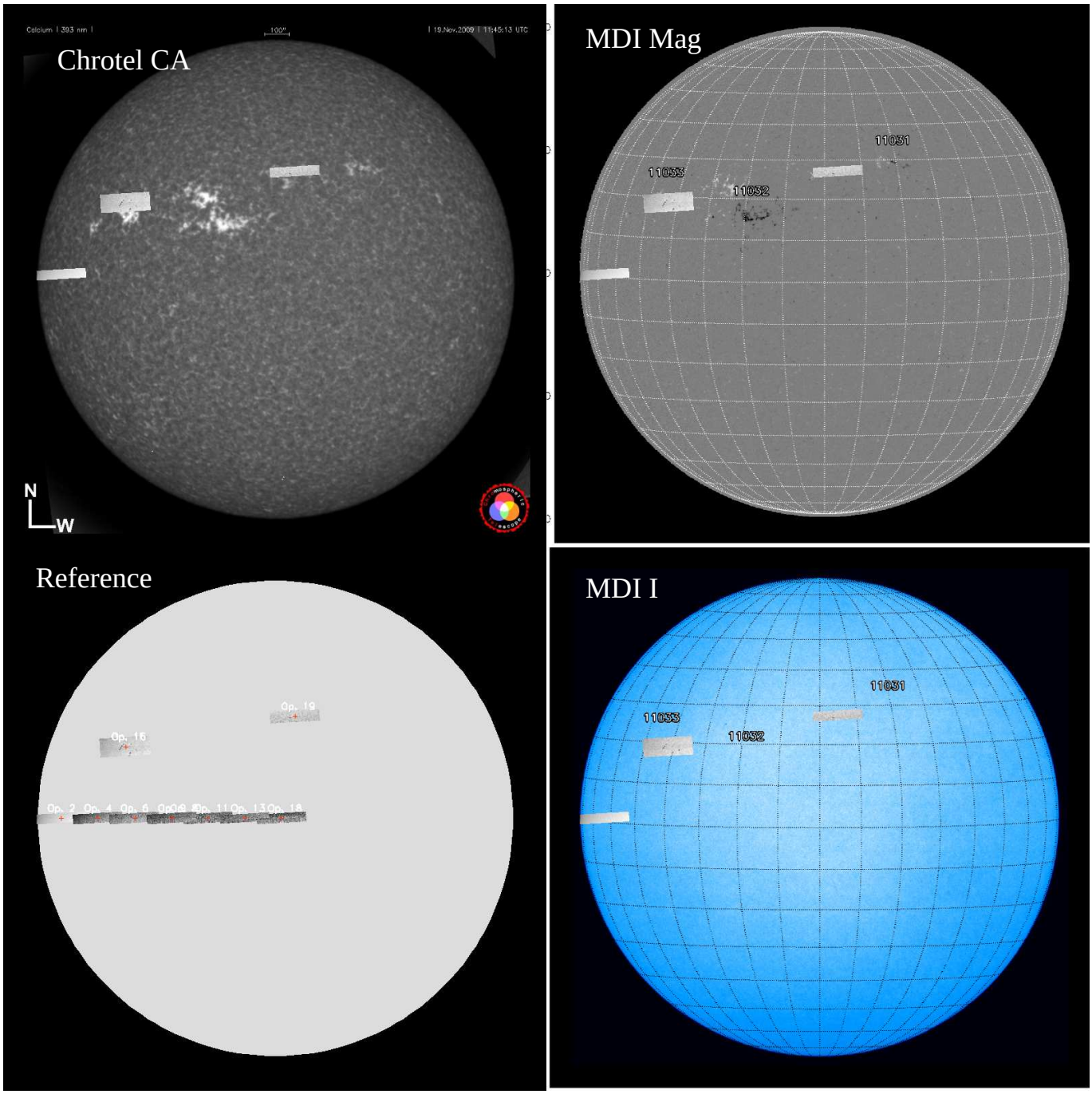

Figure 7: Same as Fig. 6, but this time overlaid over some additional full-disk images from Chrotel (*left top*), MDI magnetogram (*right top*), and MDI intensity (*right bottom*).

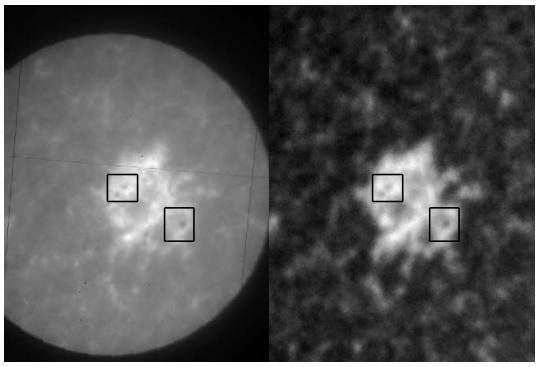

Figure 8: *Left*: Ca II K SJ image from the PCO UT 12:27. *Right*: corresponding section of the Chrotel full-disk image at UT 11:45 after rough alignment and re-scaling. The *black rectangles* outline some of darkest pores in the FOV. The slit is clearly seen as *black horizontal line*.

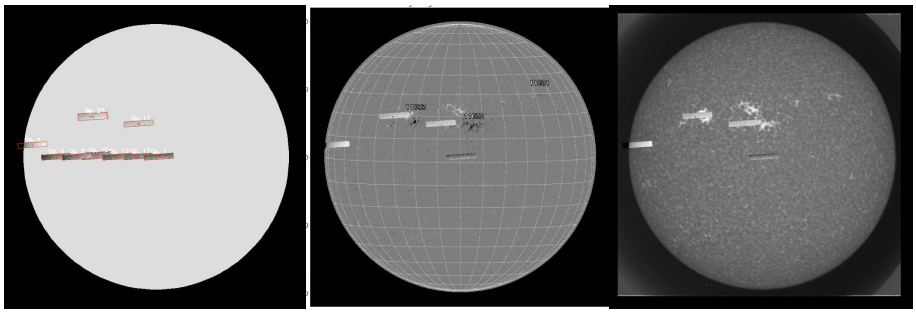

Figure 9: Location of the observed FOVs on the Sun on 20.11.09, overlaid on *left to right* the reference disk (all scans), MDI image, Chrotel image (only some of the scans).

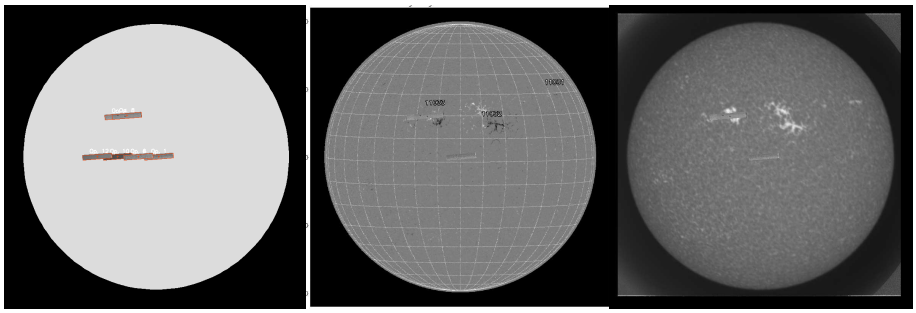

Figure 10: Location of the observed FOVs on the Sun on 21.11.09, overlaid on *left to right* the reference disk (all scans), MDI image, Chrotel image (only some of the scans).

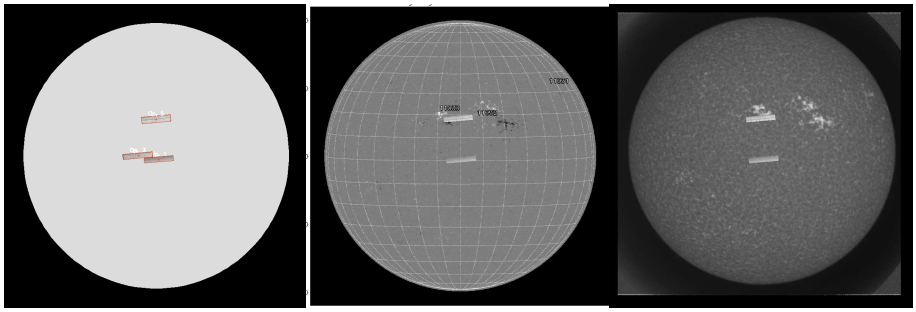

Figure 11: Location of the observed FOVs on the Sun on 22.11.09, overlaid on *left to right* the reference disk (all scans), MDI image, Chrotel image (only some of the scans).

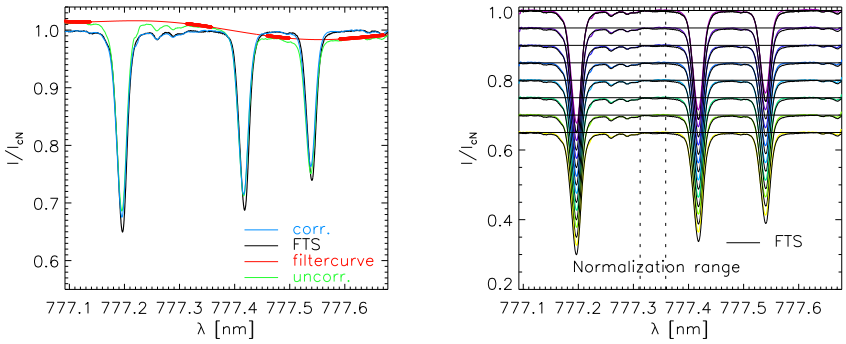

Figure 12: *Left*: average uncorrected spectrum of obs. no. 3, 19.11.09 (*green*), filtercurve (*red*), FTS spectrum (*black*), and corrected spectrum (*blue*). The continuum ranges used are marked on the filtercurve. *Right*: average profiles of all eight disc center maps on 19.11.09, 777 nm; vertically displaced for better visibility. The *vertical dashed lines* denote the range used for the intensity normalization.

5 Prefilter curve/corrections for wavelength trends

5.1 19.11.09, 777 nm

To remove additional trends of the intensity with wavelength in the data due to vignetting at the chip borders or in the predisperser focal plane, or due to the IR glass in front of the camera, a correction curve was determined (labelled "filtercurve" in the following, even if no prefilter was involved). I used the FTS atlas spectrum as reference, and determined a correction curve that modified the continuum ranges of the average observed profile of the observation no. 3 on 19.11.09 to resemble the FTS profile (*left panel* of Fig. 12). The filtercurve was constructed by first fitting a 4th order polynomial to the continuum ranges that are marked on the filtercurve. A division of the observed profile with this polynomial still showed significant deviations from the FTS. I thus fitted another polynomial of 5th order to the residuals between FTS and the profile after the first correction. The filtercurve was then defined as the product of the two polynomials.

To test the quality of the correction, the filtercurve was then applied to all eight disc center maps of the 19.11.09. The *right panel* of Fig. 12 shows the average corrected profiles of the maps vs. the FTS profile. The time of the observation increases from top to bottom; this reveals a slight temporal trend in the profile shape. Near the upper limit of the wavelength window used for determining the intensity normalization coefficient (*vertical black dashed lines*), the intensity of the observed profiles exceeds the FTS intensity by a slightly varying amount. Since the spectral shape of the FTS is, however, well matched (for instance the three weak lines from 777.25 nm to 777.3 nm), I would not start to complicate the calculation by using a time-dependent filtercurve, or to determine the filtercurve profile-by-profile.

5.2 557 nm, 20.11.09-22.11.09

For the 557 nm range, the same approach as in the previous section was chosen. I used the average profile of the observation no. 3 on 20.11.09 in this case, and determined the filtercurve again in two steps. The first step was a 4th order polynomial to continuum ranges in the profile like before. The second step was slightly different. After division with the 4th order polynomial, the continuum intensity at the red end was at unity, whereas the FTS spectrum clearly shows values below 1. To improve the correction, I manually added a straight line with a small slope to the correction curve to obtain the final filtercurve (see the *left column* of Fig. 13; the *red curve* is slightly above the original profile (*green*) at larger wavelengths). I used the same filtercurve derived form a data set on 20.11.09 for all following days; this seems to be fine. Note that there is slight deviation between the FTS profile and all corrected average profiles just to the blue of 557.7 nm, where the FTS has an a bit higher intensity. In case this is relevant/critical for the abundance determination, the filtercurve can be modified to obtain a better match near 557.7 nm, instead of trying to get a good match for the whole observed wavelength range.

With the filtercurves now defined, all intensity normalization curves were re-calculated for consistency; the shape of the curves did naturally not change, the values changed by $\ll 5\%$. The wavelength window for determining the normalization value was also optimized to correspond to a region with least influence of spectra lines. The application of the filtercurve to the data is always done after the Fourier filtering.

Important: using the FTS as reference can have introduced a bias/error, if the FTS profile has spurious small-scale variations of the continuum level of non-solar origin. It would be best to get a synthetic profile with as many lines as possible included for comparison, but I would expect no

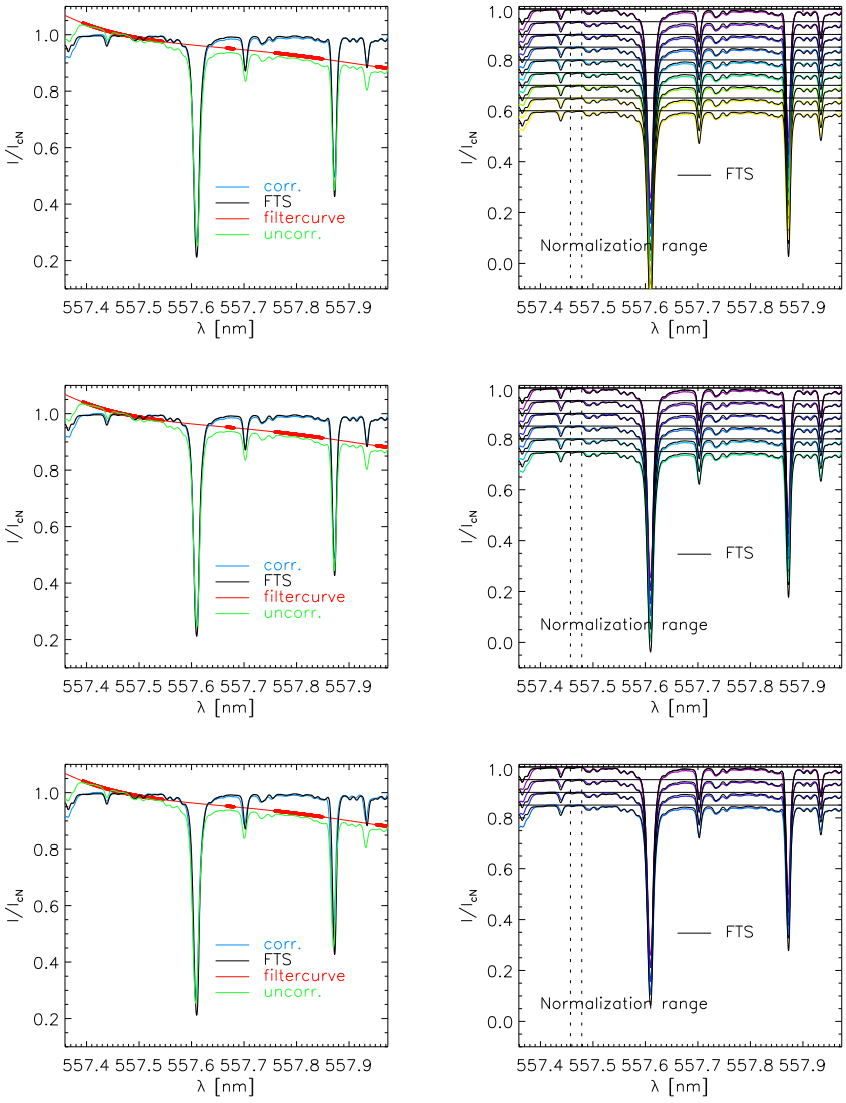

Figure 13: Same as Fig. 12 for 557 nm and for all days from 20.11. to 22.11.09 (*top to bottom*).

significant modification because of this.

6 Spectrograph resolution

The spectra taken with the main spectrograph of the VTT show a broadening due to the limited spectral resolution. There are two contributions to the broadening from the instrumental side due to the resolving power and the finite slit width.

6.1 Resolving power

The resolving power R of a spectrograph (see for instance http://www.horiba.com/us/en/scientific/products/optics-tutorial/, or ask Thomas Kentischer (TK)) is given by the product of the spectral order n, in which the observations were done, and the number of illuminated grooves, m, by

$$\frac{\lambda}{\Delta\lambda} \equiv R = n \cdot m\,. \tag{2}$$

The diameter of the pupil image on the grating is about 250 mm (TK). Since the grating is inclined by about its blaze angle of $\alpha = 63.43°$ to the light beam, the illuminated length l on the surface of the grating is given by $l = h/\cos\alpha \approx 560$ mm. With the grating constant γ of the VIS grating of 79 grooves/mm, this yields about m_{max}=44.150 illuminated grooves. The pupil image on the grating, however, is elliptical with the two semi-axes having 125 mm and 280 mm length, respectively. Thus only $\pi/4 \cdot 250 \cdot 560\,\mathrm{mm}^2 \approx 78\%$ of the full area is illuminated. As first order approximation (TK), the number of illuminated grooves then is $m = 0.78 \cdot m_{max} = 34.680$. This yields a resolving power of 1.422.000 for 557 nm (n=41), and 1.005.720 for 777 nm (n= 29). The minimal wavelength that can be resolved thus is $\Delta\lambda_{res} = 0.388$ pm@557 nm and 0.766 pm@777 nm.

6.2 Finite slit width

The physical slit width limits the maximal achievable resolution to the width of the image of the slit in the final focal plane. The physical width is changed by the magnification of the spectrograph, M:

$$M = \frac{\cos\alpha}{\cos\beta} \cdot \frac{L_{exit}}{L_{ent}}\,, \tag{3}$$

where α is the angle of incidence, β the angle of reflection, L_{exit} the length of the exit arm (7.5 m), and L_{ent} the length of the entrance arm (15 m). For the Echelle spectrograph $\alpha = \beta$ and thus $M = 1/2$. The maximal spectral resolution can then be retrieved by multiplying the size of the image of the slit with the linear dispersion d in the final focal plane. The linear dispersion in nm/mm can be calculated by

$$d = 10^6 \cdot \frac{\cos\beta}{n\,\gamma\,L_{exit}}\,, \tag{4}$$

which yields 0.0269 nm/mm@777 nm and 0.019 nm/mm@557 nm. For a comparison of the observed spectra with the FTS atlas, the linear dispersion was determined as 0.0257 nm/mm@777 nm and 0.0171 nm/mm@557 nm; in the following, I will use the latter numbers. The slit width of 40μm then corresponds to $\Delta\lambda_{slit} = 40/2 \cdot 0.0257$ pm= 0.514pm@777 nm and 0.342 pm@557 nm. The spectral sampling of 0.464 pm@777 nm and 0.307 pm@557 nm was finer than the slit-limited resolution, thus the latter provides the limit.

The total instrumental broadening can then be assumed as Gaussian profile of a width σ_{total} from the addition of the two contributions by

$$\sigma_{total} = \sqrt{\Delta\lambda_{res}^2 + \Delta\lambda_{slit}^2}\,, \tag{5}$$

which yields $\sigma_{total} = 0.922$ pm@777 nm and 0.517 pm@557 nm, corresponding to FWHM of 2.17 pm@777 nm and 1.22 pm@557 nm.

For comparison, the thermal broadening for oxygen at 6000 K has a FHWM of about 4.6 pm@777 and a macroturbulent velocity of 1 kms^{-1} produces a FHWM of 1.8 pm@777 nm. All these three contributions together yield a FWHM

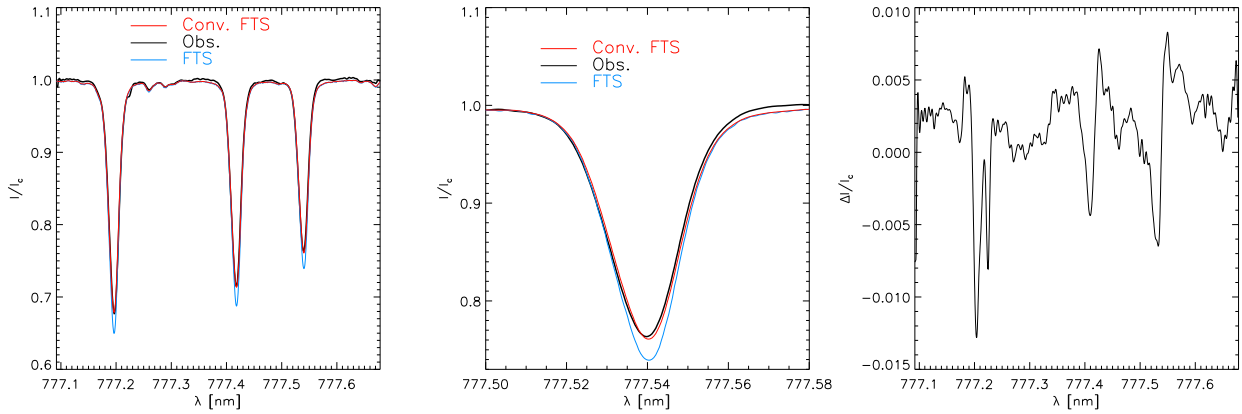

Figure 14: Convolution of FTS spectrum to observed profile. *Left*: full spectral range; FTS (*blue*), observed profile (*black*), convolved FTS (*red*). *Middle*: magnified section of spectrum. *Right*: residual differences $I_{\mathrm{FTS}}^{\mathrm{conv.}} - I_{\mathrm{obs}}$.

of 11.8 pm@777 nm, whereas the FWHM of the oxygen line in the observations or the FTS atlas is about 20 pm. Allende Prieto et al. 2004 give a broadening by 15.1 pm from spectrograph resolution + additional macro/microturbulent velocities; with another 4.6 pm from thermal broadening, this meets the 20 pm.

Before deciding for sure on the correctness of my calculation above, I would like to have some synthetic profile for test purposes (best including some FeI lines as well). The numbers for the spectrograph may be underestimated, since for instance optical aberrations are not included. Sorry, at present I can't guarantee more than that this are the theoretical numbers.

7 Stray light correction

The line depth of the observed spectral lines is slightly smaller than that of the FTS spectrum (see Fig. 1). This can be due to either the spectral resolution or stray light inside the spectrograph. Any stray light contamination caused by the optics in front of the slit *cannot change* the line depth, since it only introduces a (spatially varying) contribution of a solar profile that contains all spectral lines with the full line depth. The only light sources in front of the slit that could change the line depth are the lamps in the observing room. Since the observations were done from the main control room of the VTT in the ground floor, actually no lights at all were switched in the relevant are, leaving only the first cited two sources.

Following Allende Prieto et al. (2004), the stray light and resolution effects can be estimated by convolving the FTS profile I_{FTS} to match the observed profile I_{obs} using

$$I_{\mathrm{FTS}}^{\mathrm{conv.}} = \frac{I_{\mathrm{FTS}} + \alpha}{1 + \alpha} \otimes G(\sigma)\,, \tag{6}$$

where α measures the stray light level, and $G(\sigma)$ is a Gaussian with a suited width σ.

The quality of the choice of α and σ can be easily quantified by calculating

$$\chi^2 = \int (I_{\mathrm{FTS}}^{\mathrm{conv.}} - I_{\mathrm{obs}})^2(\lambda)\, d\lambda\,. \tag{7}$$

The calculation is straightforward and thus easily done. Figure 14 shows the result for the least χ^2 case when convolving the FTS spectrum to the observed profile. The best-fit parameters were $\alpha = 7.52$ % and $\sigma = 1.41$ pm, as marked with a *white cross* in the χ^2-surface shown in the *left panel* of Fig. 15. The χ^2 was calculated using the full observed wavelength range in Eq. (7) to be unbiased by a specific spectral line. The *middle panel* of Fig. 14 shows a magnification of the spectral line at 777.54 nm for better visibility. The convolved FTS matches well to the line depth of the observed profile, but shows some deviation at the continuum level to the red of the line. The *right panel* shows that the deviations between $I_{\mathrm{FTS}}^{\mathrm{conv.}}$ and I_{obs} are generally less than 1%, where the strongest differences in the regions of the spectral lines may also partly come from a mismatch in the two wavelength scales that affects the line width.

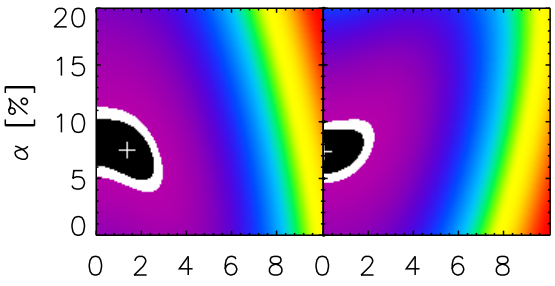

Figure 15: χ^2-surface as function of the width σ (x-axis) and the stray light level α (y-axis) for the convolution of the FTS spectrum to the observed profile (*left*) and vice versa (*right*).

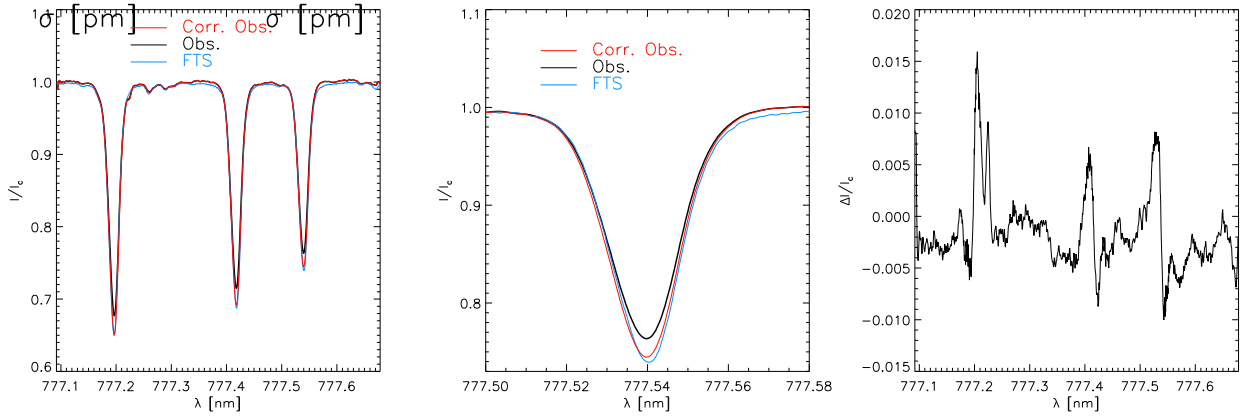

Figure 16: Same as Fig. 14 but for matching the observed profile to the FTS spectrum. *Left*: full spectral range; FTS (*blue*), observed profile (*black*), corrected observed profile (*red*). *Middle*: magnified section of spectrum. *Right*: residual differences $I_{\rm obs}^{\rm corr.} - I_{\rm FTS}$.

Since the value of σ is actually so small, especially compared with other broadening contributions (see the previous section), that it can be nearly neglected, I also used Eq. (6) in the reverse direction to "convolve" the observed profile to the FTS spectrum by changing to -α in Eq. (6). The "convolution" also only consisted in the correction by the stray light level, since the smallest χ^2 value naturally arises for $\sigma \equiv 0$ pm in this case (*right panel* of Fig. 15). The best-fit value of α was 7.38 % in this case. Figure 16 shows the comparison between the original FTS and the corrected observed profile in the same style as in Fig. 14. The residual differencesare very similar to those for the convolution of the FTS.

From the direct comparison of the FTS and observed spectra, I would conclude that we have reached the same spectral resolution as the FTS atlas. In my opinion, the stray light correction can be done in two equivalent ways: correcting the observed spectra for about 7.4% of stray light by subtraction (simple offset, no convolution), or adding the same stray light level to any synthetic spectra that are compared with the observations.

Important: if the stray light level is only due to scattering inside the spectrograph, the value to be subtracted/added is NOT 7.4% of I_c, but proportional to the light level of the respective spectrum, i.e. 7.4% of the average intensity of the spectrum in a continuum wavelength range. The correction thus should be applied on a spectrum-by-spectrum base.

Add-on: stray light calculation for 557 nm gave $\alpha = 0\%$ and σ=2.15 pm for the convolution of FTS to the observations, and $\alpha = 2\%$ for the other direction. Note that the conversion of the observations to FTS using only the stray light offset is not able to reach the FTS. For this wavelength, it seems that basically only the convolution with the Gaussian is needed.

8 First order estimate of CLV

777 nm, 19.11.09 With the positions determined from the VTT positioning information, a preliminary CLV spectrum of the 777 nm range was retrieved. I used 100 bins in $\mu = \cos\theta$, and averaged all spectra falling in the range $[k, k+1] \cdot 0.1$. The spectra were corrected for the fringes by the Fourier method described above. The filtercurve was not applied. Each spectrum was shifted spectrally to have the spectral line at 777.2 nm at a fixed reference position to

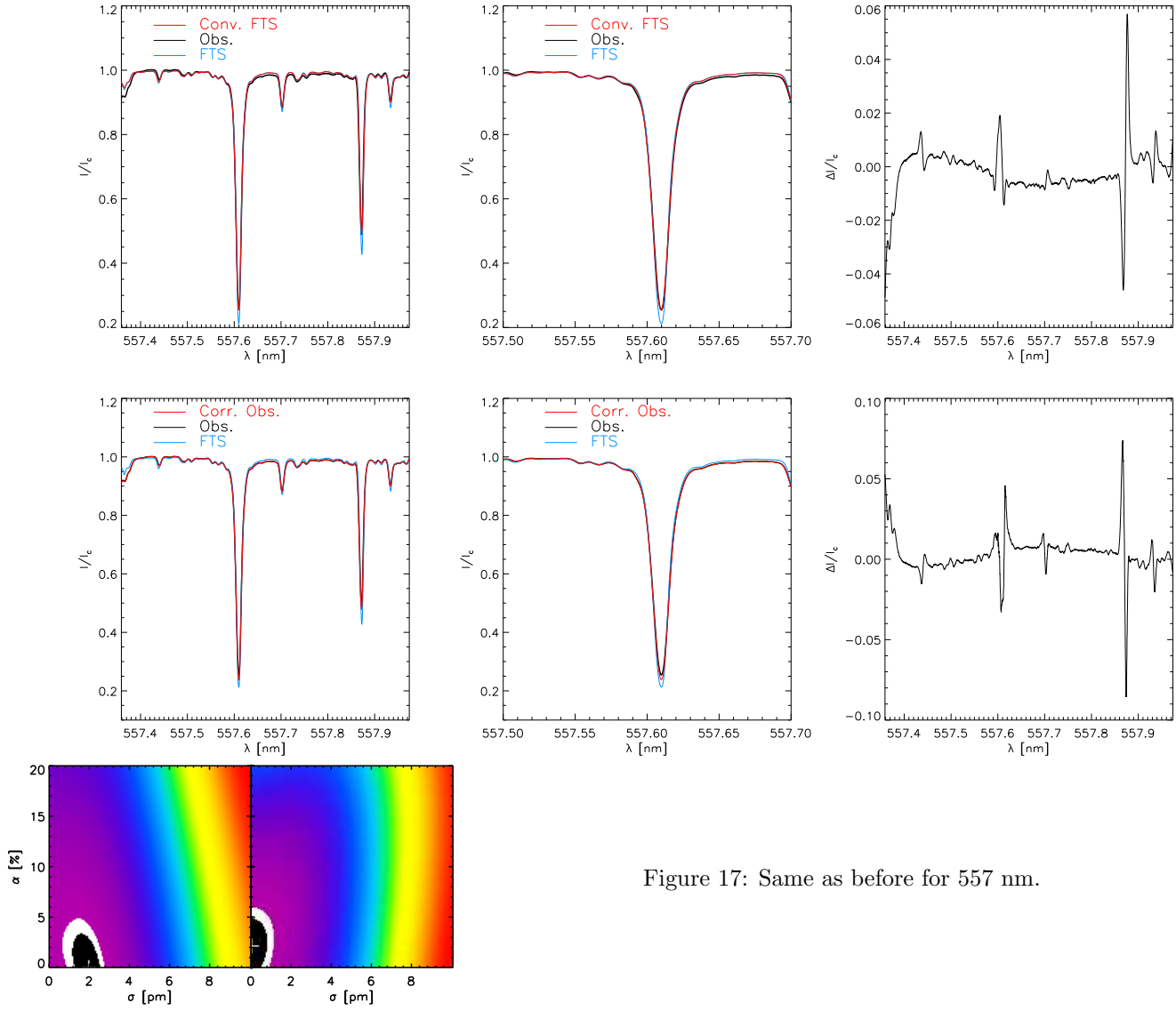

Figure 17: Same as before for 557 nm.

remove the Doppler shifts prior to averaging. The spectra were normalized to the continuum intensity at disc center at the same moment of time as they were observed with the intensity normalization value shown in Fig. 5. No further corrections were applied (wavelength trend, stray light correction). The complete available FOV was used, without excluding network areas or faculae, but the two active region observations were not included. The resulting complete CLV spectrum is displayed in Fig. 18. On first look, the only prominent features is a broadening of the lines near the very limb that is strongest for 777.2 nm.

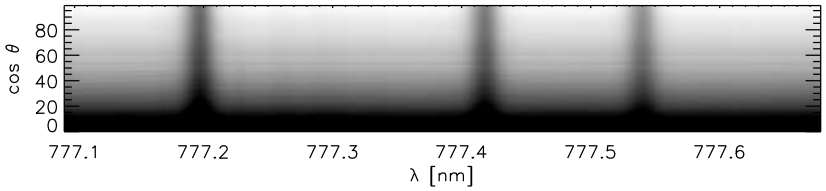

Figure 18: Average CLV spectra of the 777 nm range on 19.11.09. The limb is at bottom, disc center at top.

The number of profiles per bin is shown in the *left panel* of Fig. 19. Up to $\mu \approx 0.5$, about 10000 spectra are covered by each bin; from $\mu \approx 0.3$ to the limb, the number reduces to less than 5000 profiles. The *middle panel* shows individual spectra at some heliocentric positions. The *bottom profile* for $\mu = 0$ seems actually to be already beyond the limb because of the inaccuracy in the position values, this could be optimized manually. On first look, no clear variation with position can be seen in the spectral shape. The *right panel* shows the intensity at four wavelengths, passing from the continuum to the line core of the 777.2 nm line. The slope of the intensity curves varies. The relative line depth, $I_c - I_{\rm core}/I_c\,(\mu)$, seems to vary linearly with heliocentric position (*purple curve at bottom*).

557 nm, 20.-22.11.09 Figures 20 and 21 show the corresponding plots for the CLV of the 557 nm range. The number of profiles is comparable; the only directly visible major difference is that the line depth of the FeI at 557.6 nm has a much smaller slope with heliocentric angle.

Add-on: application of the filter curve was added to the CLV routine now (see Fig. 22).

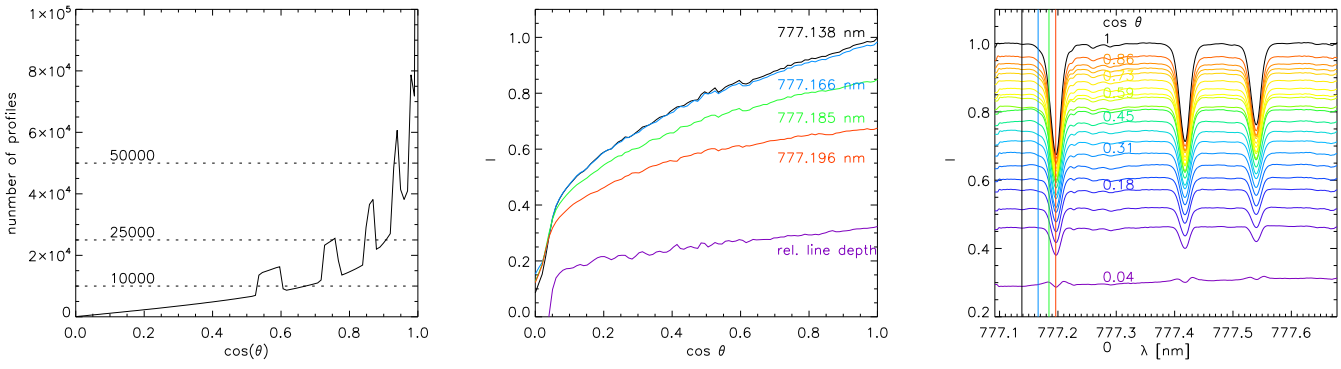

Figure 19: *Left to right*: number of profiles per bin, intensity variation at four wavelengths, spectra at some heliocentric positions given by the respective numbers. The wavelengths used for the *middle panel* are marked with *vertical lines* of the same color in the *right panel*.

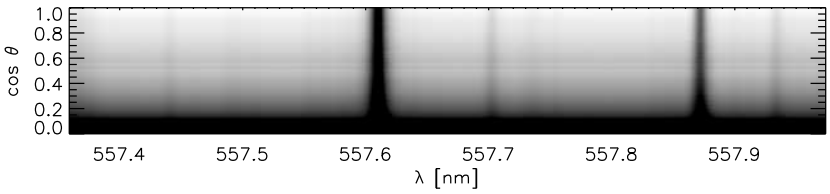

Figure 20: Average CLV spectra of the 557 nm range. The limb is at bottom, disc center at top.

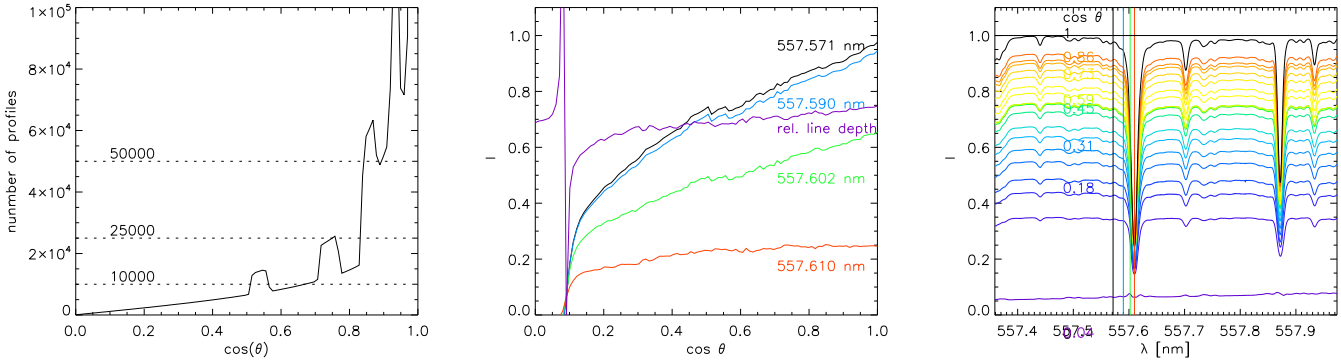

Figure 21: *Left to right*: number of profiles per bin, intensity variation at four wavelengths, spectra at some heliocentric positions given by the respective numbers. The wavelengths used for the *middle panel* are marked with *vertical lines* of the same color in the *right panel*.

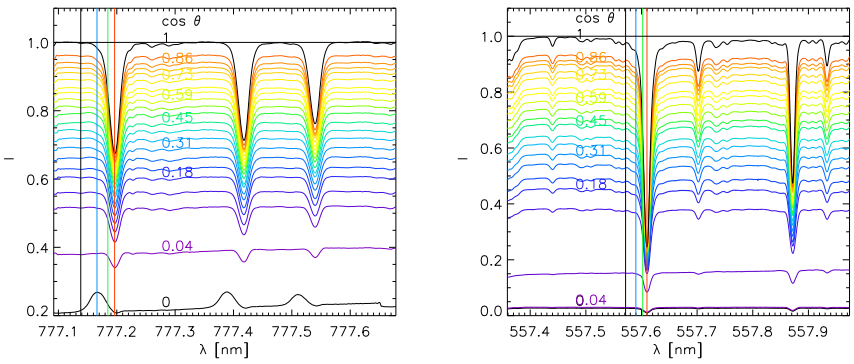

Figure 22: CLV run for 777/557 nm with the filtercurve correction (*left/right*). The spectra beyond/at the limb seem to be over-corrected for 777 nm.

9 Summary & Conclusions

The data properties can be summarized like this:

- The spectral resolution is comparable to the FTS atlas.
- The spectral sampling is sufficient to resolve the spectrograph resolution of the VTT.
- The spectral broadening by instrumental effects in the spectrograph is a factor of 2-3 below the thermal line width.
- The spectra can be corrected well for fringes and wavelength trends to an accuracy/deviation from FTS $\ll$1%.
- The stray light level is around 7.5%; a correction for this can be applied to either the observed spectra or any synthetic profiles before comparison. For using the spatially resolved spectra, it would be better to correct the stray light level in the observations (for any inversion or similar).
- An accurate normalization to disc center continuum intensity can be provided for every step of each map.
- Position values as provided by the VTT pointing system are accurate to 10-20", this only makes problems at large heliocentric angles.
- The positions were fixed by an offset determined in the map *at the limb* that covers all points up to $\mu \approx 0.5$. The error thus is now larger for the maps near disk center, where it is presumably negligible for μ.
- The data could be aligned accurately to MDI, using the PCO Ca SJ images and the full-disk Chrotel Ca images. This will be only done on additional request.
- The coverage of heliocentric positions is complete for both wavelengths; additional active region maps are available. The statistics is at least about 5000 profiles per bin of 0.1 in μ up to $\mu = 0.4$; at the very limb, the number reduces to ≈ 200 (= number of scan steps per map).
- Network masks can be defined for all FOVs from the PCO Ca SJ images.
- Granule/intergranule masks can be defined from the intensity maps of the observations themselves.

All retrieved information and the spectra themselves are stored in IDL save files for easy usage. I already collected all routines used during the data reduction. The code can be re-run with different settings for the stray light correction using implemented keywords; it needs, however, some hours each for both the intensity normalization and the CLV routine due to the sheer size of the data files ($>$ 1 GB). If necessary, it should be run on a 8GB RAM machine or similar, my desktop machine (4GB RAM) starts swapping, if other processes with even only moderate memory usage are run in parallel.

10 To be done

The following (maybe incomplete) list of tasks is still to be done:

- Define exact stray light correction method. This will also change slightly again the intensity normalization, but the routines are prepared to be re-run with additional settings.
- Finalize the reduction routines, show Damian how to use them, then he can start playing around. At present, only two routines are needed to calculate a) the intensity normalization, b) the positions. Everything else is already part of the scientific analysis (masks of network, granules, IGLs, averaging, etc.) that I would gladly hand over to Damian or whomever else.

A Complete list of observations

Table 2: Overview of observations at 777 nm.

Name	Scan area	time	position	status	comment
15.11.2009, 777 nm					
target	52 x 0.18"	-	-	reduced	
target_1	130 x 0.18"	-	-	reduced	both targets in same reduce file
obs	30 x xx"	-	-	reduced	
16.11.2009, 777 nm					
obs1	230 x 0.18"	12:05 ?	disc center	reduced	half of map with good seeing
obs2	199 x 0.18"	12:25 ?	-230/450 - 10E/30N	reduced	AR, bad seeing
17.11.2009, 777 nm					
target	199x0.18"	9:15	-	reduced	
SJ_map171109.0.sav	145	-	-		SJ images of target
stray_limb	30x0.18"	-	limb	reduced	limb not reached
stray_limb1	61x0.18"	-	limb	reduced	limb not reached, off-limb
stray_limb2	61x0.18"	-	limb	reduced	limb reached, FOV partly blocked
SJ_map171109.1.sav	140	-			SJ images limb (?)
SJ_map171109.2.sav	122	-			SJ images limb (?)
SJ_map171109.3.sav	261	-			SJ images disc center (?)
obs1	199x0.18"	10:35	center	reduced	
obs2	46x0.18"	10:53	-150/8	reduced	bad seeing
19.11.2009, 777 nm					
obs1	199	9:00	0/0	reduced	
obs2	199	9:20	-900/10	reduced	AO jump at 162
obs3	11	9:42	0/0	reduced	
obs4	199	9:48	-750/0	reduced	
obs5	11	10:05	0/0	reduced	
obs6	199	10:15	-601/0	reduced	
obs7	11	10:32	0/0	reduced	
obs8	15	10:35	-398/0	reduced	aborted
obs9	199	10:40	-448/0	reduced	
obs10	11	11:00	0/0	reduced	
obs11	199	11:07	-300/0	reduced	
obs12	11	11:25	0/0	reduced	
obs13	167	11:30	-150/0	reduced	
obs14	11x0.18"	11:45	0/0	reduced	
obs15	201x0.36"	-	-640/291	reduced	AR; CA SJ saturated
obs16	201x0.36"	12:20	-637.5/292	reduced	AR
obs17	11x0.18"	12:40	0/0	reduced	
target	199	-	-	reduced	
obs18	16	14:55	0/0	reduced	
obs19	241	-	55/416	reduced	
obs20	11	15:20	0/0	reduced	

Table 3: Overview of observations at 557 nm.

Name	Scan area	time	position	status	comment
19.11.2009, 557 nm					
target	199	-	-	reduced	AO locked at 135
obs1	199	-	disc center	reduced	
20.11.2009, 557 nm					
obs1	199	-	0/0	reduced	tip-tilt only
obs2	265	-	-485/295	reduced	AR
obs3	11	9:05	0/0	reduced	
obs4	199	-	-924/87	reduced	tip-tilt only
obs5	11	9:25	0/0	reduced	
obs6	199	9:30	-750/0	reduced	
obs7	11	9:40	0/0	reduced	
obs8	199	9:45	-599/0	reduced	
obs9	11	9:50	0/0	reduced	
obs10	261	9:55	-454/9	reduced	62 timing lost
obs11	11	10:10	0/0	reduced	
obs12	199	10:15	-303/0	reduced	
obs13	199	10:25	-150/2	reduced	
obs14	11	10:35	0/0	reduced	
obs15	265	-	-479/298	reduced	AR
obs16	11	10:50	0/0	reduced	
obs17	199	11:00	-148/243	reduced	AR
obs18	11	-	0/0	reduced	
21.11.2009, 557 nm					
obs1	199	8:50	0/0	reduced	
obs2	199	9:05	-150/0	reduced	
obs3	11	9:12	0/0	reduced	
obs4	199	9:14	-288/295	reduced	AR; SJ missing
obs5	11	9:28	0/0	reduced	
obs6	199	9:35	-150/0	reduced	good seeing
obs7	11	9:42	0/0	reduced	
obs8	199	9:50	-234/299	reduced	AR
obs9	11	10:00	0/0	reduced	
obs10	199	10:05	-300/0	reduced	
obs11	11	10:10	0/0	reduced	
obs12	199	10:20	-450/0	reduced	
22.11.2009, 557 nm					
obs1	199	9:03	5/-27	reduced	
obs2	19	-	-	reduced	aborted
obs3	199	-	-155/0	reduced	
obs4	11	9:35	0/0	reduced	
obs5	265	9:40	-20/267	reduced	pore
obs6	11	9:55	0/0	reduced	
obs7	199	10:00	-152/0	reduced	
obs8	11	10:08	0/0	reduced	

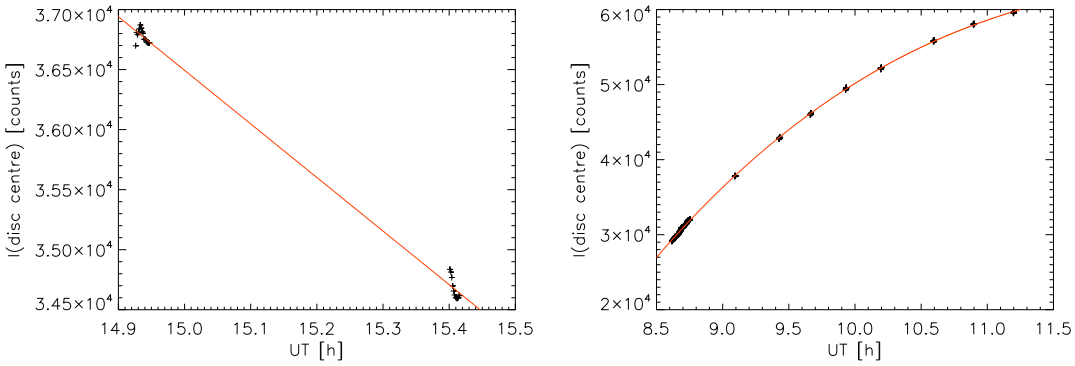

Figure 23: Intensity normalization curve for the 19.11.09 in the afternoon (*left*) and for the 20.11.09 (*right*).

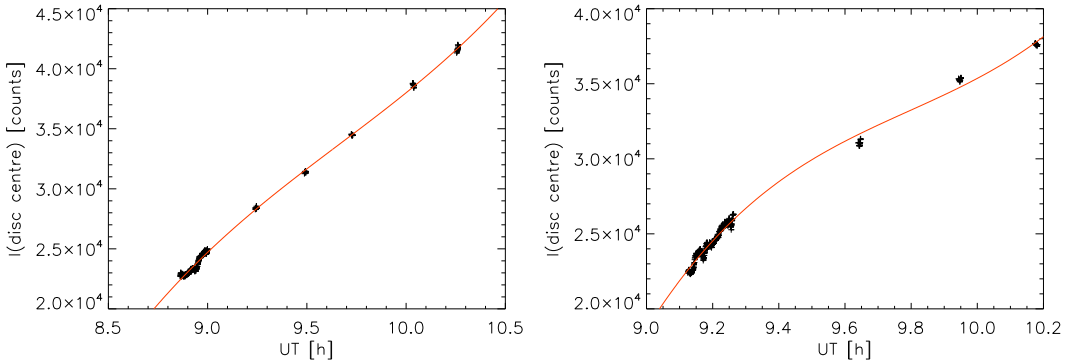

Figure 24: Intensity normalization curve for the 21.11.09 (*left*) and for the 22.11.09 (*right*).

B Intensity normalization curves